How do climate modes shape the chlorophyll-a interannual variability in the tropical Atlantic?

Fanny Chenillat, Serena Illig, Julien Jouanno, Founi Mesmin Awo, Gael Alory, Patrice Brehmer

How do climate modes shape the chlorophyll-*a* interannual variability in the tropical Atlantic?

Chenillat F.[1,2]*, S. Illig[1,3], J. Jouanno[1], F. M. Awo[3,4,5], G. Alory[1] and P. Brehmer[2,6]

[1]LEGOS, CNES/CNRS/IRD/UPS, Toulouse, FRANCE

[2]IRD, Univ Brest, CNRS, IFREMER, LEMAR, IRD DR Ouest, Plouzané, FRANCE

[3]Department of Oceanography, MARIS Institute, University of Cape Town, Cape Town, Rondebosch, SOUTH AFRICA

[4]Nansen-Tutu Centre for Marine Environmental Research, Department of Oceanography, University of Cape Town, Cape Town, Rondebosch, SOUTH AFRICA

[5]ICMPA, Université d'Abomey Calavi, Cotonou, BENIN

[6]IRD, Univ Brest, CNRS, IFREMER, LEMAR, CSRP, Dakar, SENEGAL

*corresponding author: fanny.chenillat@ird.fr

Key points (3 – 140 characters each):

- The leading Tropical Atlantic climate modes shape the spatio-temporal variability of the Cold Tongue interannual surface Chlorophyll-*a*.
- The Atlantic Zonal Mode explains the interannual Chlorophyll-*a* variability in the eastern part of the Cold Tongue with a peak in summer.
- The North Tropical Atlantic mode influences the interannual Chlorophyll-*a* variability in the western Cold Tongue, from spring to winter.

Keywords

Tropical Atlantic; Equatorial Atlantic; Cold Tongue; chlorophyll-*a* concentration; interannual variability; Climate modes; Remote sensing.

Abstract

Chlorophyll-*a* concentration (Chl-a) observed by satellite shows a marked seasonal and interannual variability in the Tropical Atlantic. This study analyzes how the remotely-sensed surface Chl-a responds to the leading boreal summer climate modes affecting the interannual Tropical Atlantic variability over 1998-2018, corresponding to a positive Atlantic Multidecadal Oscillation phase. We show that the Atlantic Zonal Mode (AZM) and the North Tropical Atlantic Mode (NTAM) significantly drive the interannual surface Chl-a variability in the equatorial Atlantic, with different timings and contrasted zonal modulation of the Cold Tongue. The AZM involves remotely-forced wave propagations favoring upwelling in the east and Chl-a modulation in the core of the Cold Tongue. Instead, the impact of the NTAM is mainly in the west, in response to locally-forced pumping that modulates the western extension of the Cold Tongue. Such conditions can affect the marine food web, inducing significant variations for ecosystem functioning and fisheries.

Plain language summary

The Tropical Atlantic Ocean is characterized by strong year-to-year surface temperature fluctuations which can be classified into basin-scale climate modes. In this study, we examine to which extent these modes of variability have a signature on the surface Chlorophyll-a concentration, a proxy of the biological activity at sea. Using two decades (1998-2018) of ocean-color satellite observations, we show that the interannual surface Chlorophyll-a modulation in boreal summer is impacted by these climate modes mainly along the equator. They drive contrasted Chlorophyll-a fluctuations in time and space. The first climate mode, the Atlantic Zonal Mode, involves distant mechanisms that propagate along the equator favoring biological activity in the eastern equatorial basin. Conversely, the second mode, the North Tropical Atlantic Mode, involves local mechanisms in the west of the equatorial band where it favors biological activity. Such conditions can affect the marine food web, inducing significant variations for the fisheries.

1. Introduction

The tropical Atlantic is characterized by a low-frequency variability of coupled ocean-atmosphere processes leading to extreme events with critical societal impacts (high rainfall, drought, hurricane; Foltz et al., 2019). These fluctuations which mainly concern the Sea Surface Temperature (SST), occur at different time-scales, from interannual to multidecadal - for the Atlantic Multidecadal Oscillation, AMO (Kerr 2000; Knight et al. 2006). The interannual variability is governed by two leading climate modes, namely the Atlantic Zonal Mode (AZM) and the North Tropical Atlantic Mode (NTAM) (Xie & Carton, 2004; Foltz & McPhaden, 2010). The AZM, also known as the Atlantic Niño or the Atlantic equatorial mode, is associated in its positive phase with anomalous warming (cooling in its negative phase) of boreal summer SST confined to the eastern equatorial basin (**Fig.S1a**; Kushnir et al., 2006; Lübbecke et al., 2018). In contrast, the NTA, also known as the Atlantic Meridional Mode or Dipole mode, is characterized by an interhemispheric gradient of SST Anomalies (SSTA), with anomalous warm conditions in the north tropical Atlantic region and weak negative SSTA south of the equator during its positive phase, and conversely during its negative phase (**Fig.S1b**; Chiang and Vimont, 2014). This interannual mode modulates the latitudinal position of the Atlantic Intertropical Convergence Zone (ITCZ) (e.g., Xie & Carton, 2004). The NTAM usually peaks in boreal spring (Kushnir et al., 2006) and, notably, still has a signature in boreal summer (Richter et al., 2013). The imprint of these two interannual modes is directly modulated by the multidecadal variability, namely the AMO as shown in Martin-Rey et al. (2018). In particular, Vallès-Casanova et al. (2020) investigated the diversity of the Atlantic Niños and showed significant variations of the onset and duration of the SSTA they attributed to preconditioning driven by external forcing such as NTAM or Pacific El Niño.

This interannual variability of the tropical Atlantic is likely to impact the marine ecosystem. SST variability can indeed reflect the modulation of nutrient inputs through the thermocline depth displacements and result in the variability of chlorophyll-*a* concentration (Chl-a) and marine ecosystems. Actually, in such a region where there is no light-limitation at the surface, the primary production is predominantly driven by the nutrient availability in response to physical drivers (Longhurst, 1993; Longhurst, 2007). To our knowledge, the most extensive investigation of seasonal and interannual variability of Chl-a in the tropical Atlantic was carried out by Grodsky et al. (2008), using a 10-year-long time-series of sea surface Chl-a. Using an updated 21-year-long time-series of remote-sensed surface Chl-a (see Material &

Methods), we confirm their results (Figs.1ab): the richest surface waters are located along the coasts due to coastal upwelling and river discharges and also in the equatorial Atlantic Cold Tongue region where the equatorial upwelling prevails Seasonal and interannual equatorial Chl-a variability peaks at [10˚W, 0°N], spreading zonally from 0°E to 30˚W (Fig.1a). It is maximum in boreal summer (0.35 $\pm$0.1 mg.m^{-3}, Fig.1b). Surface Chl-a anomalies in the Cold Tongue show marked interannual variability (Fig.1c). This is even more striking when looking at the zonal extension of Chl-a anomalies along the whole equatorial waveguide (Fig.1d). Interestingly, while on average surface Chl-a interannual variability peaks around 10˚W, it can extend over the whole equatorial Atlantic and peak at 25˚W (e.g., in 2002).

Grodsky et al. (2008) hypothesized that interannual variability of the sea surface Chl-a and SST in the eastern equatorial Atlantic is driven by the thermocline displacements, associated with the interannual fluctuations of the equatorial zonal wind. However, the broader effect on primary productivity is still unknown (Foltz et al., 2019). This leads us to question the sources of such temporal and spatial variability of the sea surface Chl-a on an interannual timescale in the entire equatorial Atlantic. We will focus our study on the boreal summer period when seasonal and interannual variability of Chl-a is maximum (Fig.1b). In this paper, using remote-sensed observations over the equatorial Atlantic region, we describe how interannual climate modes shape the Chl-a variability in time and space.

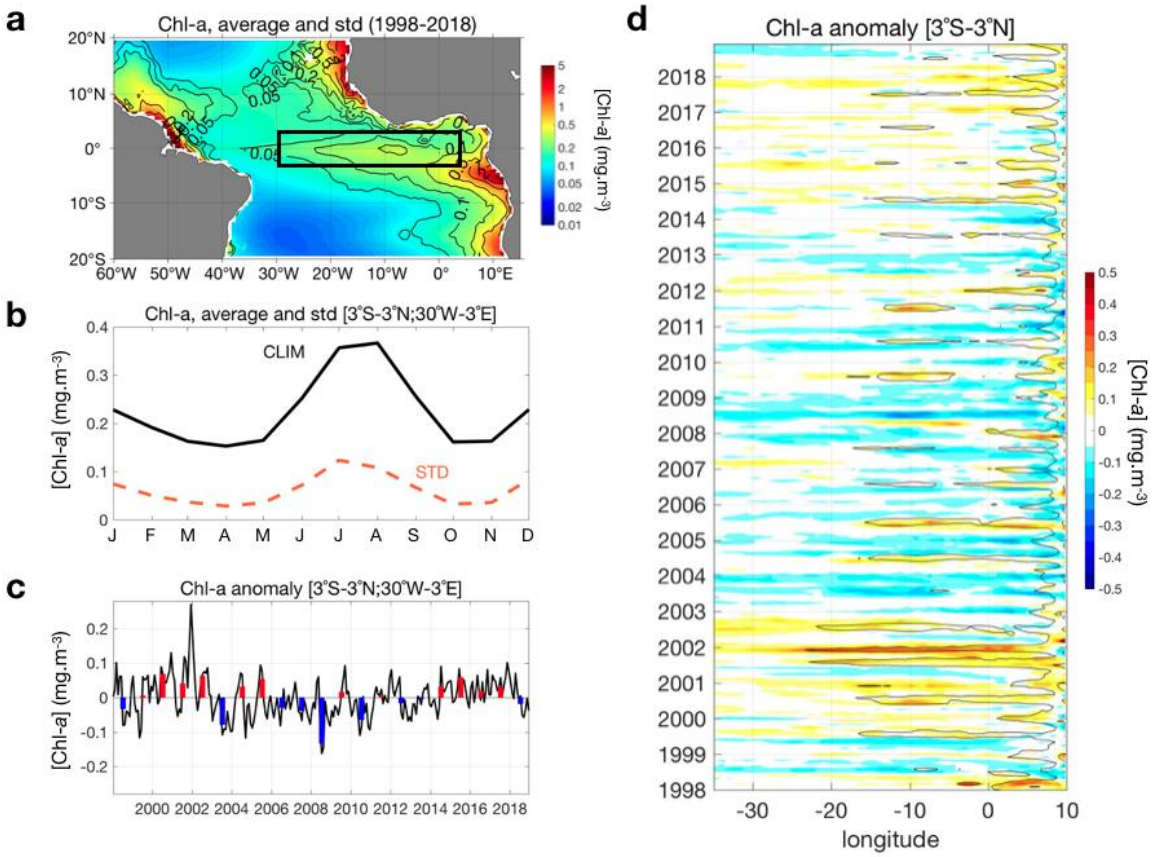

Figure 1: Temporal and spatial variability of surface chlorophyll-a concentration (Chl-a, mg.m^{-3}) from satellite observations over 1998-2018. (a) Mean (color shading) and interannual standard deviation (black contours). (b) Climatological monthly mean (black line) and interannual monthly standard deviation (STD, orange dashed line) averaged over the Cold Tongue area ([3°S-3°N; 30°W-3°E], delineated by the black box in panel a). (c) Monthly (black line) and boreal summer (June-July-August average, red/blue bars) interannual anomalies in the Cold Tongue. (d) Longitude-time Hovmöller diagram of the equatorial interannual anomalies averaged within [3°S-3°N].

2. Material and methods

This study has been conducted using ocean-color satellite data over the 1998-2018 period in the Tropical Atlantic region from 20°S to 20°N. Ocean-color, provided by E.U. Copernicus Marine Service Information, is a proxy for open-sea Chl-a (Fournier et al., 2015). We analyzed cloud-free Chl-a monthly maps (L4 product, CMEMS 2020a), based on the Copernicus-GlobColour processing chain. Concomitant monthly SST and near-surface atmospheric circulation described through zonal and meridional wind components come from the European Center for Medium-Range Weather Forecasts ERA-Interim reanalysis (Dee et al., 2011). Monthly remote-sensed Sea Surface Height (SSH), a good approximation for the

thermocline displacements, is available since 1993 from Aviso Ssalto/Duacs (Pujol et al., 2016) and provided by CMEMS (2020b).

After removing the linear trend, monthly interannual anomalies are estimated relative to the 1998-2018 climatology. We focus on the boreal summer Chl-a variability and following Martin Rey et al. (2018), we average the data over the June-July-August (JJA) season. Diagnostics consist primarily of Empirical Orthogonal Function (EOF) analyses and linear regressions. The EOF analysis allows decomposing the Tropical Atlantic SSTA variability into a set of independent spatial modes (the EOFs, **Fig.2**) associated with distinct temporal fluctuations – the Principal Components (PCs, **Figs.3ef**). Classically, PCs are normalized such as their standard deviation (STD) is 1 and the EOF spatial pattern conveys the unit of the variable. To isolate the part of the Chl-a, wind, and SSH variability associated with each leading EOF mode, we linearly regress (using a least mean square method) the interannual time-series onto the standardized PCs (**Figs.3a-d**). The goodness of the linear fit is systematically measured by the square of the correlation coefficient (r^2) between PCs and the independent time-series. Throughout the study, the statistical significance of correlations is estimated based on Student's t-test at the 95% confidence level.

Because we aim at understanding Chl-a interannual variability, we preferentially focus on anomalous productive years corresponding to the occurrence of cold interannual events. We thus present the cold phase of the leading EOF modes of the Tropical Atlantic SST, inversely to the usual convention.

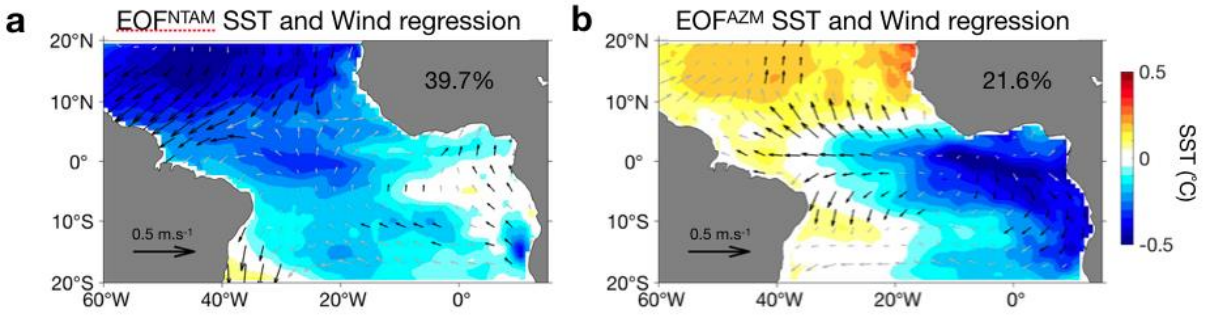

Figure 2: Maps of the two leading Empirical Orthogonal Function (EOF) of boreal summer 'June-July-August' (JJA) interannual Sea Surface Temperature (SST) variability (color shading, °C) in the tropical Atlantic ([20°S-20°N, 60°W-15°E]) over the 1998-2018 period. The percentages indicate the explained variance of each mode. JJA surface wind interannual anomalies (arrows, $m.s^{-1}$) are regressed onto the respective standardized Principal Component (PC, shown in **Fig.3ef**). Significant values (> 95% confidence level) are shown with black vectors. NTAM: North Tropical Atlantic mode. AZM: Atlantic Zonal mode.

3. Climate modes and Chl-a variability

3.1 Tropical Atlantic interannual climate modes over a positive AMO phase

As expected, two leading modes of interannual climate variability emerge from the analysis of boreal summer tropical Atlantic SSTA (Fig.2). While these patterns stray from the classical climate modes (described in the introduction; Fig.S1), they are consistent with Martin-Rey et al. (2018), who recently diagnosed a modulation of the leading climate mode structures regarding the AMO phase. These results are coherent since EOFs analyses are performed over the last two decades (1998-2018) and that the AMO is in a positive phase since the 1990s (Wu et al., 2019).

The dominant mode explains 39.7% of the summer tropical Atlantic interannual variability. It is characterized by strong northern cold (warm) SSTA, accompanied by anomalous northeasterly (southwesterly) trades, contrasting with a near-zero positive (negative) SSTA south of the equator, confined to the eastern tropical Atlantic (Fig.2a). Such pattern resembles closely the NTAM pattern during positive AMO phases (Martin-Rey et al., 2018).

The second leading mode explains 21.6% of the summer tropical Atlantic interannual variability. It is characterized by strong cold (warm) SSTA in the eastern equatorial Atlantic extending southeastwards along the African coast in the Benguela upwelling system (Fig.2b) typical of an Atlantic Niña (Niño) event. Divergent (convergent) anomalous surface winds overlie the eastern equatorial Atlantic SSTA event (Illig et al., 2020), associated with a strengthening (relaxation) of the Trade winds in the western-central equatorial Atlantic and coastal poleward (equatorward) winds along the Benguela current system. A weak interhemispheric SSTA gradient is also depicted. This pattern is typical of the AZM during positive AMO phases (Martin-Rey et al., 2018).

Note that, in comparison with Martin-Rey et al. (2018), we find that the NTAM explains more variance than the AZM mode during a positive AMO phase. This can be attributed to the temporal and spatial restriction of our analysis (Lübbecke et al., 2018), i.e., two decades over 20˚S-20˚N against 34 years over 30˚S-30˚N in Martin-Rey et al. (2018). A possible linear mix between the two climate modes (Servain et al., 1999; Hormann and Brandt, 2009) or the effect of climate change (Lübbecke et al., 2018) might also explain this difference.

3.2 NTAM and the western equatorial Chl-a modulation

The interannual SSH Anomaly (SSHA) signature associated with the cold phase of the NTAM shows negative anomalies mostly in the northern Tropical Atlantic and in the western part of the equatorial band, from 40˚W to 5˚W with a peak at 40-30˚W (**Fig.3a**). Considering the SSH as a proxy for the thermocline depth (Arnault et al., 1992), a cold-phase NTAM is mainly associated with a shoaling of the thermocline where negative SSHA are located (Martin-Rey et al., 2018). Such a thermocline rise is likely to be driven locally by a positive Ekman Pumping anomaly associated with the increased surface wind-stress curl (**Fig.S2**). In the western equatorial sector, the shoaling of the thermocline is expected to enhance the equatorial upwelling and therefore increase the vertical nutrients flux into the euphotic layer and enhance the Chl-a in the surface layer. This mechanism is consistent with the Chl-a signature associated with the cold phase of the NTAM (**Fig.3c**). Positive Chl-a anomalies are indeed observed in the western part of the equatorial fringe collocated with the SSHA. They extend zonally from 40˚W to 15˚W with a peak near ~25˚W. Such a close link between SSHA and Chl-a patterns suggests control of Chl-a by vertical processes, though vertical nutrient fluxes. There is, however, no significant modulation of the Chl-a anomalies in the northern Tropical Atlantic (5-15°N), despite the significant productivity occurring yearlong (**Fig.1a**). The apparent weak sensitivity of surface Chl-a in this region to climate modes would deserve further attention.

Consistently, the interannual modulation of NTAM (PC^{NTAM}) and the Chl-a averaged in the Cold Tongue region have a correlation of 0.41. Notably, this correlation substantially increases and becomes statistically significant when only the western part of the Cold Tongue (CTW) is considered (r=0.64, >99%) (**Fig.3e**), with a regression coefficient of -0.12 $mg.m^{-3}$/°C. Conversely, the eastern Cold Tongue Chl-a variability is not correlated with PC^{NTAM}. Hence, the NTAM mode significantly explains the interannual boreal summer Chl-a variability in the western equatorial band with strong positive anomalies in 2002 and 2015 and negative anomalies in 2010 (also visible in **Figs.1cd**). Interestingly, 2002 has been investigated by Hormann and Brandt (2009). They diagnosed 2002 as an abnormally warm year in the eastern part of the Cold Tongue contrasting with cold anomalies in the western part (west of 25˚W), similarly to our cold-phase NTAM pattern (**Fig.1a**).

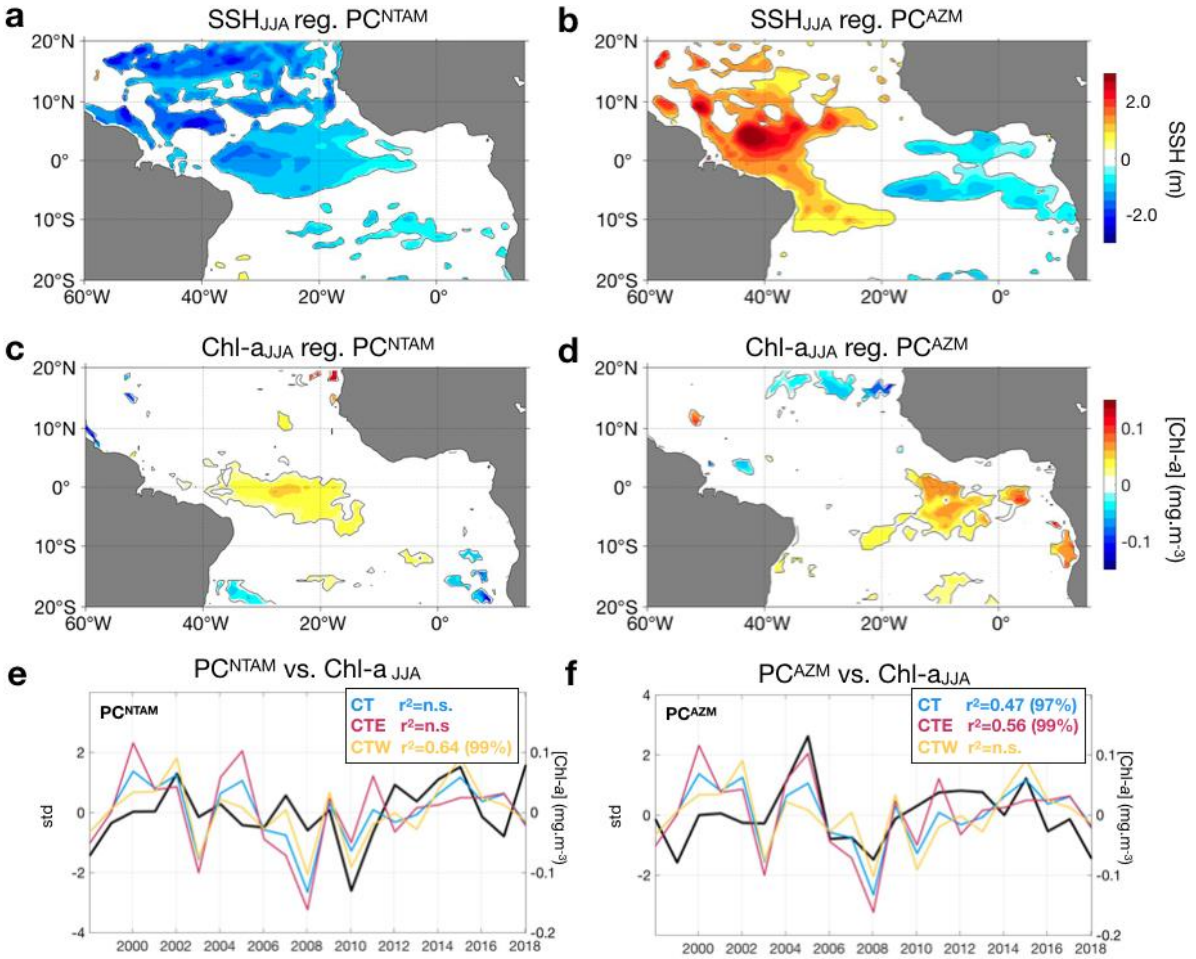

Figure 3: Spatio-temporal characteristics of the boreal summer (JJA) Sea Surface Height (SSH) and Chl-a associated with the NTAM and AZM interannual EOF modes of the Tropical Atlantic SST (presented in **Fig.2**). Regression maps of JJA SSH interannual anomalies (cm) onto the NTAM (a) and AZM (b) standardized Principal Components (PCs, shown in panels e-f (black lines)). Only significant values (> 95% confidence level) are shaded. (c-d) Same as panels a-b for JJA Chl-a anomaly (mg.m^{-3}). NTAM (e) and AZM (f) EOF PCs (black lines) are compared with boreal summer surface Chl-a interannual anomalies averaged in different portions of the Cold Tongue: entire Cold Tongue (CT, [3˚S-3˚N; 27˚W-3˚E], blue lines), eastern Cold Tongue (CTE, [3˚S-3˚N; 15˚W-3˚E], pink lines), and western Cold Tongue (CTW, [3˚S-3˚N; 27˚W-15˚W], orange lines). Squared correlation (r^2) and associated significance level (%) quantify the goodness of the linear fit between PCs and Chl-a time-series. n.s.: not significant

3.3 AZM and the eastern equatorial Chl-a modulation

The cold phase of the AZM is associated with strong positive interannual SSHA in the western Tropical Atlantic, from 10˚S to ~15-20˚N, which contrasts with the negative SSHA in the Gulf of Guinea (east of 20˚W) (**Fig.3b**). The latter are divided into two SSH depressions nearly symmetric about the Equator and centered ~4°-5° of latitude away from the Equator, typical of the signature of equatorial Rossby waves on the SSH. These upwelling waves are most likely associated with the reflection of eastward-propagating equatorial Kelvin waves

forced earlier in the western equatorial basin by the zonal wind fluctuations associated with the AZM (Illig et al. 2004) (**Fig.2b**). Incidentally, part of the equatorial Kelvin wave energy could also have been transmitted along the African coast as coastally-trapped waves, which would explain the remaining negative SSHA depicted off Angola (Bachèlery et al., 2020). These interannual SSHA fluctuations reflect a substantial shoaling (deepening) of the thermocline in the eastern (western) tropical Atlantic. The rise of the thermocline would yield a positive nutrient advection into the sunlit layer and should explain the positive surface Chl-a anomalies in the eastern Cold Tongue and along the southern Angola Current (**Fig.3d)**.

The interannual modulation of the AZM (PC^{AZM}) (**Fig.3f**) and the Chl-a averaged in the whole Cold Tongue region are significantly correlated (r=0.47, >95%). This correlation slightly increases when only the eastern part of the Cold Tongue is considered (r=0.56, >99%), with a regression coefficient of -0.10 $mg.m^{-3}$/°C, while the western Cold Tongue Chl-a variability is not correlated with PC^{AZM}. Therefore, we conclude that the AZM interannual climate mode significantly explains the interannual boreal summer Chl-a variability in the eastern equatorial band with a strong positive event in 2005 and a negative event in 2008 (also visible in **Figs.1cd**). Hormann and Brandt (2009) have also analyzed the abnormally cold year of 2005. In contrast to 2002, during the boreal summer of 2005, the easterlies were stronger in the western basin, and the Equatorial Under Current was embedded in a shallower thermocline at 23˚W. The thermocline was abnormally shallow in the whole eastern equatorial Atlantic (Marin et al., 2009) and was associated with a weak equatorial Kelvin wave activity. Vallès-Casanova et al. (2020) classified the year 2005 as a La Niña event, characterized by an early onset and persistent cold anomalies along the equator, peaking at 10˚W in June.

3.4 Spatio-temporal modulation under NTAM and AZM influence.

To diagnose the spatio-temporal modulation of the surface properties by the two leading climate modes, we linearly regress the 3-month running-mean of SST, surface wind, SSH, and Chl-a interannual anomalies onto the standardized PC^{NTAM} and PC^{AZM} (**Fig.3ef**). **Fig.4** presents a longitude-time Hovmöller diagram of the regression coefficients averaged in the equatorial band for the NTAM and AZM. A coherent longitude-time evolution of the key equatorial properties anomalies emerges for both modes and can be interpreted in the light of the climatological conditions (**Fig.S3**).

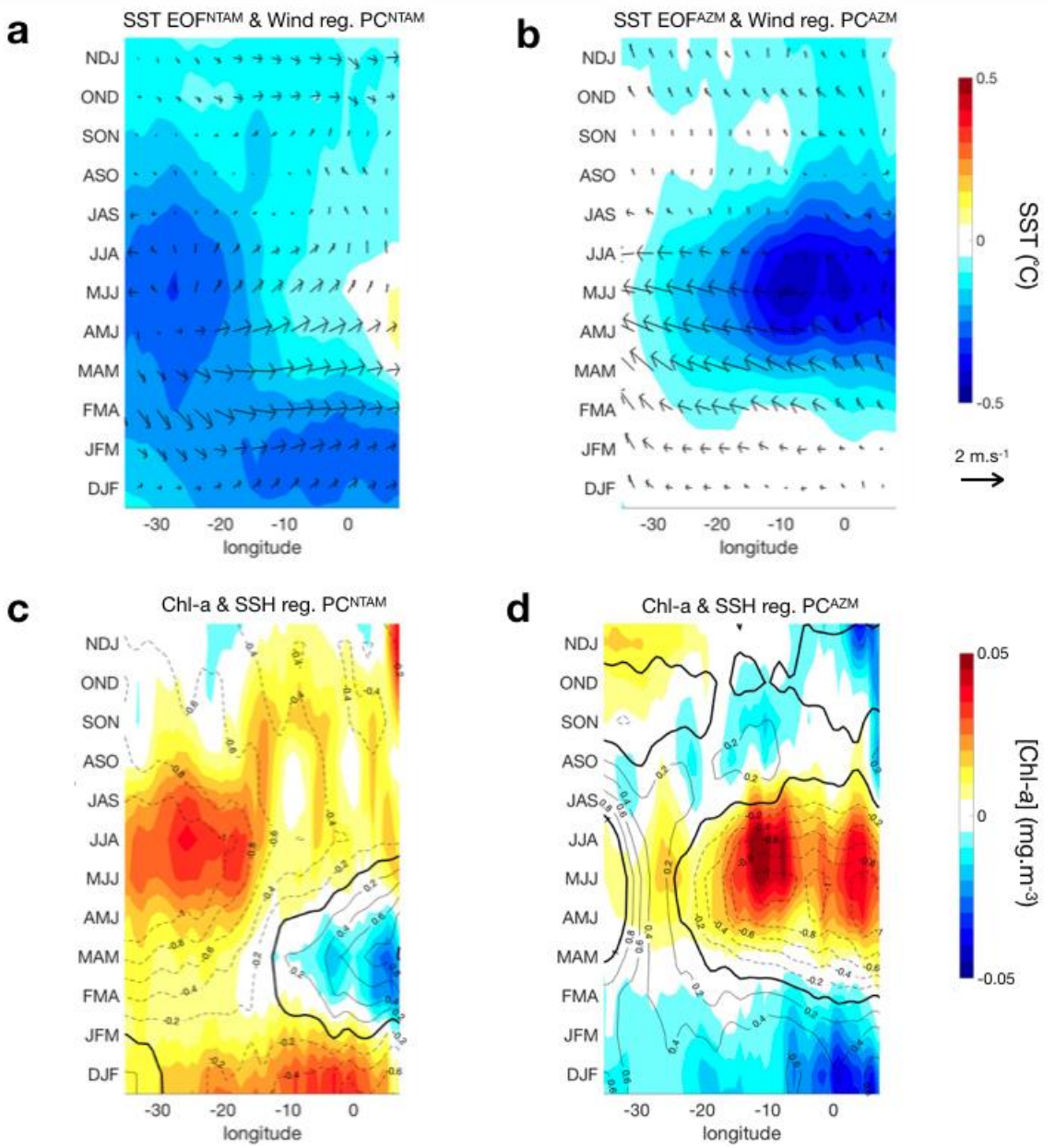

271 **Figure 4**: Phenology of equatorial surface properties associated with NTAM (left panels) and
272 AZM (right panels) EOF modes of JJA interannual Tropical Atlantic SSTA. 3-month running-
273 mean of SST, surface wind, SSH, and Chl-a interannual anomalies from preceding winter (DJF)
274 to following winter (NDJ) are regresses onto the standardized PCs (shown in **Fig.3ef**) and
275 averaged within [3˚S-3˚N]. SSTA (color shading, °C) and surface winds anomalies (arrows, m.s^{-1})
276 associated with JJA NTAM and AZM are displayed on top panels. On bottom panels, same
277 for Chl-a (color shading, mg.m^{-3}) and SSH (contours, cm) interannual anomalies.
278

279 For the NTAM, the cold phase is associated with a cold equatorial SSTA in the western
280 basin, that progresses from the end of the boreal winter. It extends from the Brazilian coast
281 to ~15˚W and peaks in early boreal summer (MJJ) at ~30˚W, concomitant with anomalous
282 wind divergence (**Fig.4a**). Collocated with this cold event in the western equatorial Atlantic,
283 **Fig.4c** discloses a strong and persistent negative SSHA and a positive Chl-a anomaly in boreal

summer (MJJ and JJA). These physical and biogeochemical anomalies are concomitant and steady, which suggests that they are associated with local vertical processes consistent with the increased Ekman pumping diagnosed from the NTAM anomalous surface wind-stress curl (Fig.S2). Concurrently, from boreal winter (JFM) to early summer (MJJ), relaxed easterlies are observed along the whole equatorial band. They drive downwelling equatorial Kelvin waves which reduce the equatorial upwelling in the eastern basin, leading to a strong zonal seesaw pattern in SSH, SST, and Chl-a anomalies. Note that Hormann and Brandt (2009), who studied a typical NTAM year (2002), also associated such a cold event with abnormally relaxed easterlies in the western basin. They emphasized a strong Equatorial Under Current core embedded in a shallow thermocline at 23˚W which is consistent with the anomalous positive Ekman Pumping triggered by the surface wind pattern discussed earlier. Interestingly, during the following boreal fall, the cold anomaly slowly progresses eastwards east of 20˚W, accompanied by a negative SSHA and a positive Chl-a anomaly. Also, the NTAM boreal summer western cold event is preceded by cold SSTA in the eastern basin in boreal winter (DJF), associated with negative SSHA and positive Chl-a anomalies. This pattern is typical of the boreal winter Atlantic Niño II mode from Okumura and Xie (2006), shown to act as preconditioning to the subsequent boreal spring NTAM.

For the AZM, the cold phase is associated with a cold equatorial anomaly extending east of ∼20˚W to the African coast. The cold event spreads slowly westwards from late winter and is maximum in early boreal summer (MJJ) at ∼10˚W (Fig.4b, coherently with La Niña pattern from Vallès-Casanova et al., 2020). This eastern cold anomaly is driven by an intensification of easterly trades along the equator initiated in boreal winter (JFM) and persisting until the following summer (JJA) (Fig.4b). Concomitant to this cold SSTA, a strong negative SSHA and a positive Chl-a anomaly are depicted (Fig.4d). The latter can be attributed to the enhanced upwelling of cold nutrient-rich deep water into the surface layer (Radenac et al., 2020), driven by remotely-forced equatorial wave triggered by the reinforcement of easterly trades in the western-central basin. This analysis also reveals a localized moderate positive Chl-a MJJ peak at 25°W which seems to detach itself from the core eastern Chl-a anomaly and differs from the SSTA pattern. After the summer, an abrupt termination of the interannual event (Fig.4bd) is associated with an eastward propagation of moderate positive SSHA and negative Chl-a anomalies that crosses the basin in ∼2 months (from JAS to SON). The timing and characteristics of this propagation are consistent with a Kelvin wave triggered by the

316 reflection of a downwelling Rossby wave forced upstream the relaxation of the easterlies.
317 Notably, similar to the NTAM signature, an eastern negative Chl-a anomaly associated with a
318 positive SSHA are observed at the beginning of the year. They may contribute to the
319 modulation of eastern boreal winter Cold Tongue bloom (also visible in Fig.1bd; Perez et al.,
320 2005; Grodsky et al. 2008; Radenac et al. 2020). The study of the winter bloom is beyond the
321 scope of this paper, but additional attention could be given to its interannual variability in
322 future research projects.
323
324 ## 4. Concluding Remarks
325 This study aims to describe how interannual climate modes shape the Tropical Atlantic
326 Chl-a variability in time and space using a 21-year-long time-series remote-sensed
327 observations over the equatorial Atlantic region. As expected, two leading modes of
328 interannual climate variability emerge from our analysis of boreal summer (JJA) tropical
329 Atlantic SSTA: namely the AZM and NTAM. Both NTAM and AZM spatial patterns do not
330 strictly fit their canonical signature but are under the influence of a positive AMO phase
331 (1998-2018) (Martin-Rey et al., 2018).
332 We show that AZM and NTAM significantly drive the interannual surface Chl-a
333 variability in the equatorial Atlantic, with different timings and contrasted modulation in the
334 Cold Tongue. The NTAM influences preferentially the interannual Chl-a variability in the
335 western Cold Tongue, from boreal spring to fall (peaking in summer), while the AZM affects to
336 a large extend, the interannual Chl-a variability in the eastern Cold Tongue, during boreal
337 summer. Our results suggest that the significant surface wind anomalies in the western
338 equatorial Atlantic associated with each climate mode have distinct effects on the ocean
339 dynamics. The relaxation of easterlies in boreal winter associated with the cold phase of
340 NTAM yields a shoaling of the western equatorial thermocline through Ekman pumping, while
341 the AZM cold-phase intensification of easterlies in boreal spring triggers equatorial Kelvin
342 wave propagation responsible for an anomalous shoaling of the thermocline in the eastern
343 Cold Tongue region 1-2 months later. The locally- and remotely-forced vertical fluxes advect
344 nutrients into the euphotic layer and increase the primary production in the western and
345 eastern Cold Tongue region, respectively. This east/west contrast in the interannual Chl-a
346 fluctuations is confirmed by an EOF analysis on the Chl-a restricted over the 3°S-3°N
347 equatorial band (Fig.S4). The first leading mode is associated with a strong positive anomaly

along the equator (with concomitant peaks at 25, 18, and 10˚W) with a temporal modulation significantly correlated with PC^{NTAM} (r=0.53). The second leading mode highlights an east/west dipole of Chl-a anomalies (peaking at 10˚W and 30˚W, respectively) with a temporal modulation significantly correlated with PC^{AZM} (r=0.61). Additionally, similar east/west partition of the equatorial Atlantic has already been documented (Longhurst, 2007; Perez et al. 2005; Longhurst et al. 1995), but simply based on the seasonality of biogeochemical properties, discriminating the variability in the Eastern Tropical Atlantic Province and the Western Tropical Atlantic Province, associated with a large boreal summer variability and a reduced boreal autumn peak, respectively.

This work provides new insights into the interannual variability of Chl-a, and its zonal signature, in this under-explored region. The role of such climate variability on Chl-a is likely to arise a myriad of biogeochemical implications. The challenge now is to understand how these climate modes impact the interannual spatio-temporal variability of the planktonic ecosystem, their consequences on the biological carbon pump and the higher trophic levels. In-depth analyses using a coupled physical-biogeochemical model are under investigation to diagnose biological-physical processes such as advective and diffusive nutrient fluxes and their potential impact on subsurface Chl-a and plankton ecosystem dynamics.

Acknowledgements:

This work is part of the TRIATLAS European project (South and Tropical Atlantic climate-based marine ecosystem prediction for sustainable management; H2020 grant agreement No 817578) which supported a post-doc fellowship funded by Institut de Recherche pour le Développement (IRD-France). The reanalysis data were downloaded from ECMWF (http://www. ecmwf.int).

References

Arnault, S., Morliére, A., Merle, J., & Ménard, Y. (1992). Low-frequency variability of the tropical Atlantic surface topography: Altimetry and model comparison, J. Geophys. Res., 97(C9), 14259– 14288, doi:10.1029/92JC00818.

Bachèlery, ML., S. Illig & M. Rouault (2020). Interannual Coastal Trapped Waves in the Angola-Benguela Upwelling System and Benguela Niño and Niña events. Journal of Marine Systems, Vol 203, March 2020, 103262, https://doi.org/10.1016/j.jmarsys.2019.103262.

Chiang, J.C.H., Vimont, D.J. (2004). Analogous Pacific and Atlantic meridional modes of tropical atmosphere-ocean variability. J Clim. 17(21):4143–4158. https://doi.org/10.1175/JCLI4953.1

E.U. Copernicus Marine Service Information (2020a). Global ocean chlorophyll, pp and pft (copernicus-globcolour) from satellite observations: monthly and daily interpolated (reprocessed from 1997), Available at: *https://resources.marine.copernicus.eu (product id=OCEANCOLOUR_GLO_CHL_L4_REP_OBSERVATIONS_009_082)* (Accessed: 15 september 2020).

E.U. Copernicus Marine Service Information (2020b). Global ocean gridded L4 sea surface heights and derived variables reprocessed (copernicus climate service), Available at: *https://resources.marine.copernicus. (product id= SEALEVEL_GLO_PHY_L4_REP_OBSERVATIONS_008_047)* (Accessed: 20 october 2020).

Dee, D. P., Uppala, S. M., Simmons, A. J., Berrisford, P., Poli, P., Kobayashi, S., et al. (2011). The ERA-Interim reanalysis: Configuration and performance of the data assimilation system. Quarterly Journal of the Royal Meteorological Society, 137(656), 553–597. https://doi.org/ 10.1002/qj.828

Foltz, G., Brand, P., Richter, I., Rodríguez-Fonseca, B., Hernandez, F., Dengler, M., et al. (2019). The tropical Atlantic observing system. Frontiers in Marine Science, 6, 206. https://doi.org/10.3389/fmars.2019.00206

Foltz, G. R., & McPhaden, M. J. (2010). Interaction between the Atlantic meridional and Niño modes. Geophysical Research Letters, 37, L18604. https://doi.org/10.1029/2010GL044001

Fournier, S., Chapron, B., Salisbury, J., Vandemark, D., & Reul, N. (2015). Comparison of spaceborne measurements of sea surface salinity and colored detrital matter in the Amazon plume. Journal of Geophysical Research: Oceans, 120(5), 3177-3192.

Grodsky, S. A., Carton, J. A., & McClain, C. R. (2008). Variability of upwelling and chlorophyll in the equatorial Atlantic, Geophys. Res. Lett., 35, L03610, doi:10.1029/2007GL032466.

Hormann, V., & Brandt, P. (2009). Upper equatorial Atlantic variability during 2002 and 2005 associated with equatorial Kelvin waves, J. Geophys. Res., 114, C03007, doi:10.1029/2008JC005101.

Illig S, Bachèlery, M.L., & Lübbecke, J.F. (2020). Why do benguela niños lead atlantic niños? J. Geophys Res Oceans 125(9):e2019JC016003. https://doi.org/10.1029/2019JC016003

Illig, S., Dewitte, B., Ayoub, N., du Penhoat, Y., Reverdin, G., de Mey, P., Bonjean, F., & Lagerloef, G.S.E., 2004: Interannual Long Equatorial Waves in the Tropical Atlantic from a High Resolution OGCM Experiment in 1981-2000. *J. Geophys. Res. Oceans*, 109, C02022, doi: 10.1029/2003JC001771

Kerr, R. A. (2000). A North Atlantic climate pacemaker for the centuries. Science 288, 1984–1986.

Knight, J. R., Folland, C.K., & Scaife, A.A. (2006). Climate impacts of the Atlantic Multidecadal Oscillation, Geophys. Res. Lett., 33, L17706, doi:10.1029/2006GL026242.

Kushnir, Y., Robinson, W.A. , Chang, P., & Robertson, A.W. (2006). The physical basis for predicting Atlantic sector seasonal-to-interannual climate variability, J. Clim., 19, 5949 – 5970.

Lübbecke, J. F., Rodríguez-Fonseca, B., Richter, I., Martín-Rey M., M., Losada, T., Polo, I., & Keenlyside, N. S. (2018). Equatorial Atlantic variability—Modes, mechanisms, and global teleconnections. WIREs Climate Change, 9(4), e527. https://doi.org/10.1002/wcc.527

Longhurst, A. R. (1993). Seasonal cooling and blooming in tropical oceans. Deep-Sea Research 40 , pp. 2145-2165

Longhurst, A. R. (2007). Ecological Geography of the Sea, 2nd ed., Academic, Burlington, Vt.

Marin F., Caniaux, G., Giordani, H., Bourlès, B., Gouriou, Y., & Key, E. (2009). Why Were Sea Surface Temperatures so Different in the Eastern Equatorial Atlantic in June 2005 and 2006? J. Phys. Oceanogr., 39(6):1416-1431. doi:10.1175/ 2008JPO4030.1

435 Martín-Rey, M., Polo, I., Rodríguez-Fonseca, B., Losada, T., & Lazar, A. (2018). Is there
436 evidence of changes in tropical Atlantic variability modes under AMO phases in the
437 observational record? Journal of Climate, 31(2), 515–536. https://doi.org/10.1175/JCLI-
438 D-16-0459.1
439 Okumura, Y., & Xie, S. (2006). Some overlooked features of tropical Atlantic climate leading to
440 a new Niño-like phenomenon. Journal of Climate, 19(22), 5859–5874.
441 https://doi.org/10.1175/JCLI3928.1
442 Pujol, M.-I. et al. DUACS DT2014 (2016). The new multi-mission altimeter data set
443 reprocessed over 20 years. Ocean Sci. 12, 1067–1090.
444 Pérez, V., Fernández, E., Marañón, E., Serret, P., & García-Soto, C. (2005). Seasonal and
445 interannual variability of chlorophyll a and primary production in the Equatorial Atlantic:
446 in situ and remote sensing observations, J. Plankton Res., 27, 189–197.
447 Radenac, M.-H., Jouanno, J., Tchamabi, C. C., Awo, M., Bourlès, B., Arnault, S., & Aumont, O.
448 (2020). Physical drivers of the nitrate seasonal variability in the Atlantic cold tongue,
449 Biogeosciences, 17, 529–545, https://doi.org/10.5194/bg-17-529-2020.
450 Richter, I., Behera, S. K., Masumoto, Y., Taguchi, B., Sasaki, H., & Yamagata, T. (2013). Multiple
451 causes of interannual sea surface temperature variability in the equatorial Atlantic
452 Ocean. Nature Geoscience, 6(1), 43–47. https://doi.org/10.1038/ngeo1660
453 Servain, J., Wainer, I., McCreary, J. P., & Dessier, A. (1999). Relationship between the
454 equatorial and meridional modes of climatic variability in the Tropical Atlantic, Geophys.
455 Res. Letters, 26, 485-488.
456 Vallès-Casanova, I., Lee, S.-K., Foltz, G. R., & Pelegrí, J. L. (2020). On the spatiotemporal
457 diversity of Atlantic Niño and associated rainfall variability over West Africa and South
458 America. Geophysical Research Letters, 47, e2020GL087108.
459 https://doi.org/10.1029/2020GL087108
460 Xie, S-.P., & Carton, J. A. (2004). Tropical atlantic variability: Patterns, mechanisms, and
461 impacts. In C. Wang, S.-P. Xie, & J. A. Carton (Eds.), Earth's climate: The ocean-
462 atmosphere interaction, Geophysical Monograph Series (121–142). Washington, DC:
463 American Geophysical Union
464 Wu, CR., Lin, YF., Wang, YL. et al. (2019). An Atlantic-driven rapid circulation change in the
465 North Pacific Ocean during the late 1990s. Sci Rep 9, 14411.
466 https://doi.org/10.1038/s41598-019-51076-1

Acronyms:

AZM: Atlantic Zonal Mode

Chl-a: Surface Chlorophyll-a concentration

CT: Cold Tongue region ([3˚S-3˚N; 30˚W-3˚E])

CTE: Eastern Cold Tongue area ([3˚S-3˚N; 15˚W-3˚E])

CTW: Western Cold Tongue area ([3˚S-3˚N; 27˚W-15˚W])

EOF: Empirical Orthogonal Function

NTAM: North Tropical Atlantic Mode

PDF: Probability Distribution Functions

SSH: Sea Surface Height

SSHA: Sea Surface Height interannual Anomalies

SST: sea Surface Temperature

SSTA: sea Surface Temperature interannual Anomalies

STD: standard deviation

Figure 1.

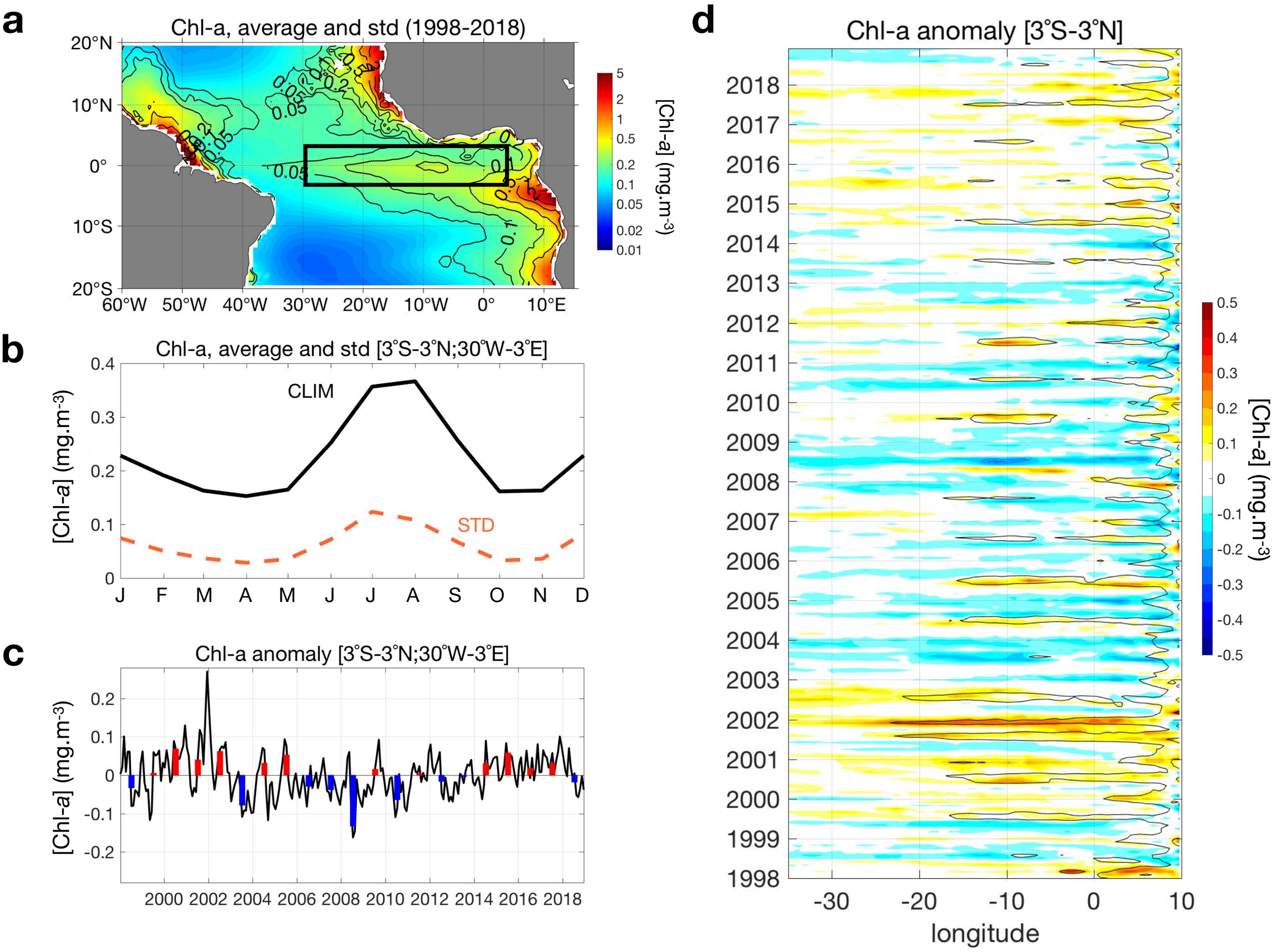

Figure 1: Temporal and spatial variability of surface chlorophyll-a concentration (Chl-a, mg.m^{-3}) from satellite observations over 1998-2018. (a) Mean (color shading) and interannual standard deviation (black contours). (b) Climatological monthly mean (black line) and interannual monthly standard deviation (STD, orange dashed line) averaged over the Cold Tongue area ([3˚S-3˚N; 30˚W-3˚E], delineated by the black box in panel a). (c) Monthly (black line) and boreal summer (June-July-August average, red/blue bars) interannual anomalies in the Cold Tongue. (d) Longitude-time Hovmöller diagram of the equatorial interannual anomalies averaged within [3˚S-3˚N].

Figure 2.

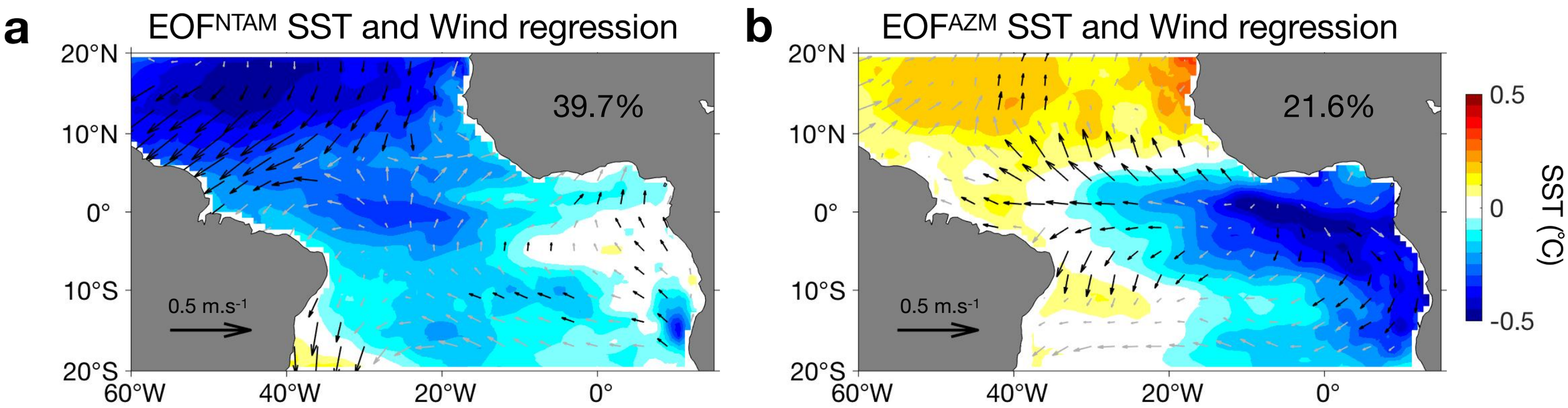

Figure 2: Maps of the two leading Empirical Orthogonal Function (EOF) of boreal summer 'June-July-August' (JJA) interannual Sea Surface Temperature (SST) variability (color shading, °C) in the tropical Atlantic ([20˚S-20˚N, 60˚W-15˚E]) over the 1998-2018 period. The percentages indicate the explained variance of each mode. JJA surface wind interannual anomalies (arrows, m.s-1) are regressed onto the respective standardized Principal Components (PC, shown in Fig.3ef). Significant values (> 95% confidence level) are shown with black vectors. NTAM: North Tropical Atlantic mode. AZM: Atlantic Zonal mode.

Figure 3.

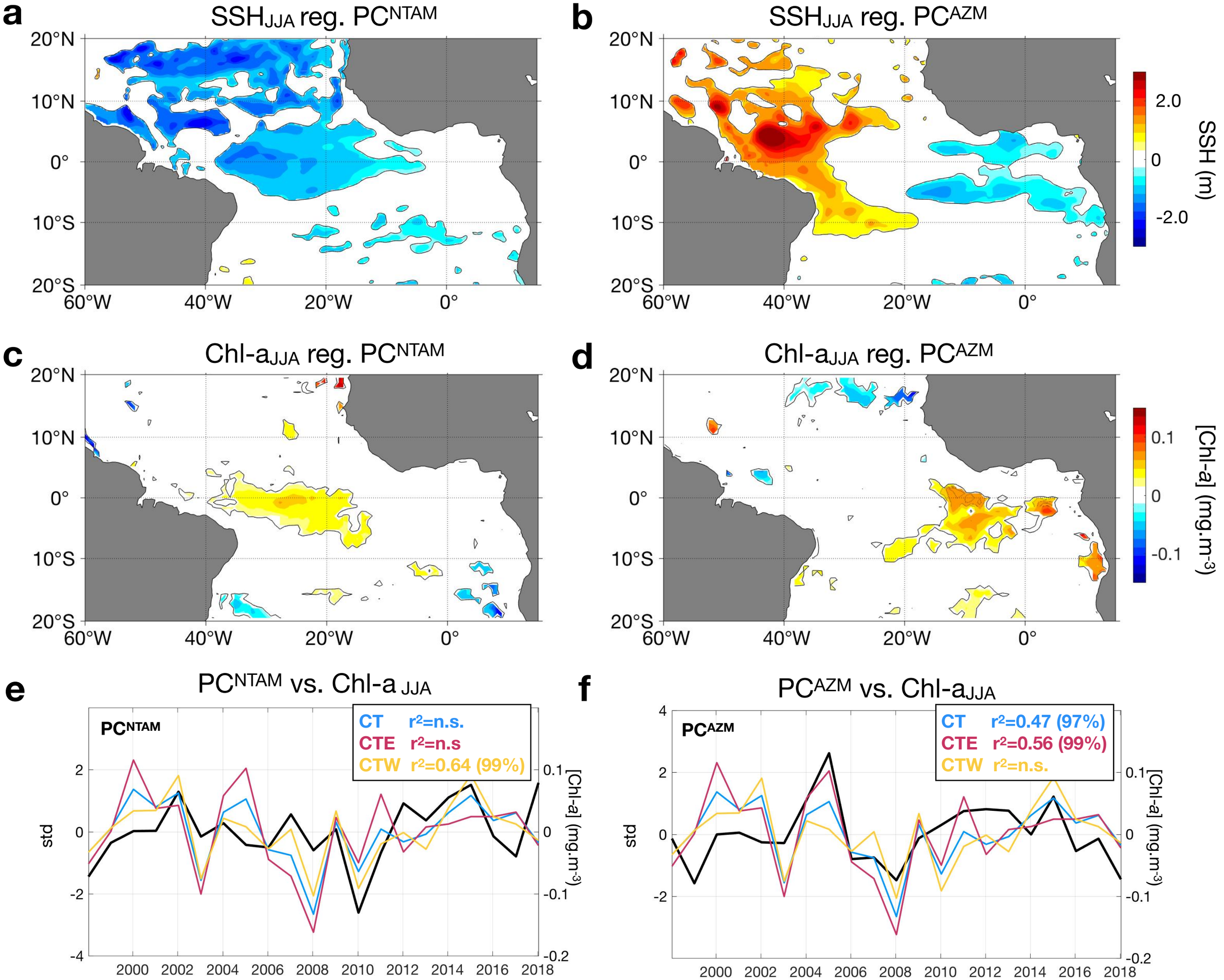

Figure 3: Spatio-temporal characteristics of the boreal summer (JJA) Sea Surface Height (SSH) and Chl-a associated with the NTAM and AZM interannual EOF modes of the Tropical Atlantic SST (presented in Fig.2). Regression maps of JJA SSH interannual anomalies (cm) onto the NTAM (a) and AZM (b) standardized Principal Components (PCs, shown in panels e-f (black lines)). Only significant values (> 95% confidence level) are shaded. (c-d) Same as panels a-b for JJA Chl-a anomaly (mg.m-3). NTAM (e) and AZM (f) EOF PCs (black lines) are compared with boreal summer surface Chl-a interannual anomalies averaged in different portions of the Cold Tongue: entire Cold Tongue (CT, [3˚S-3˚N; 27˚W-3˚E], blue lines), eastern Cold Tongue (CTE, [3˚S-3˚N; 15˚W-3˚E], pink lines), and western Cold Tongue (CTW, [3˚S-3˚N; 27˚W-15˚W], orange lines). Squared correlation (r2) and associated significance level (%) quantify the goodness of the linear fit between PCs and Chl-a time-series. n.s.: not significant

Figure 4.

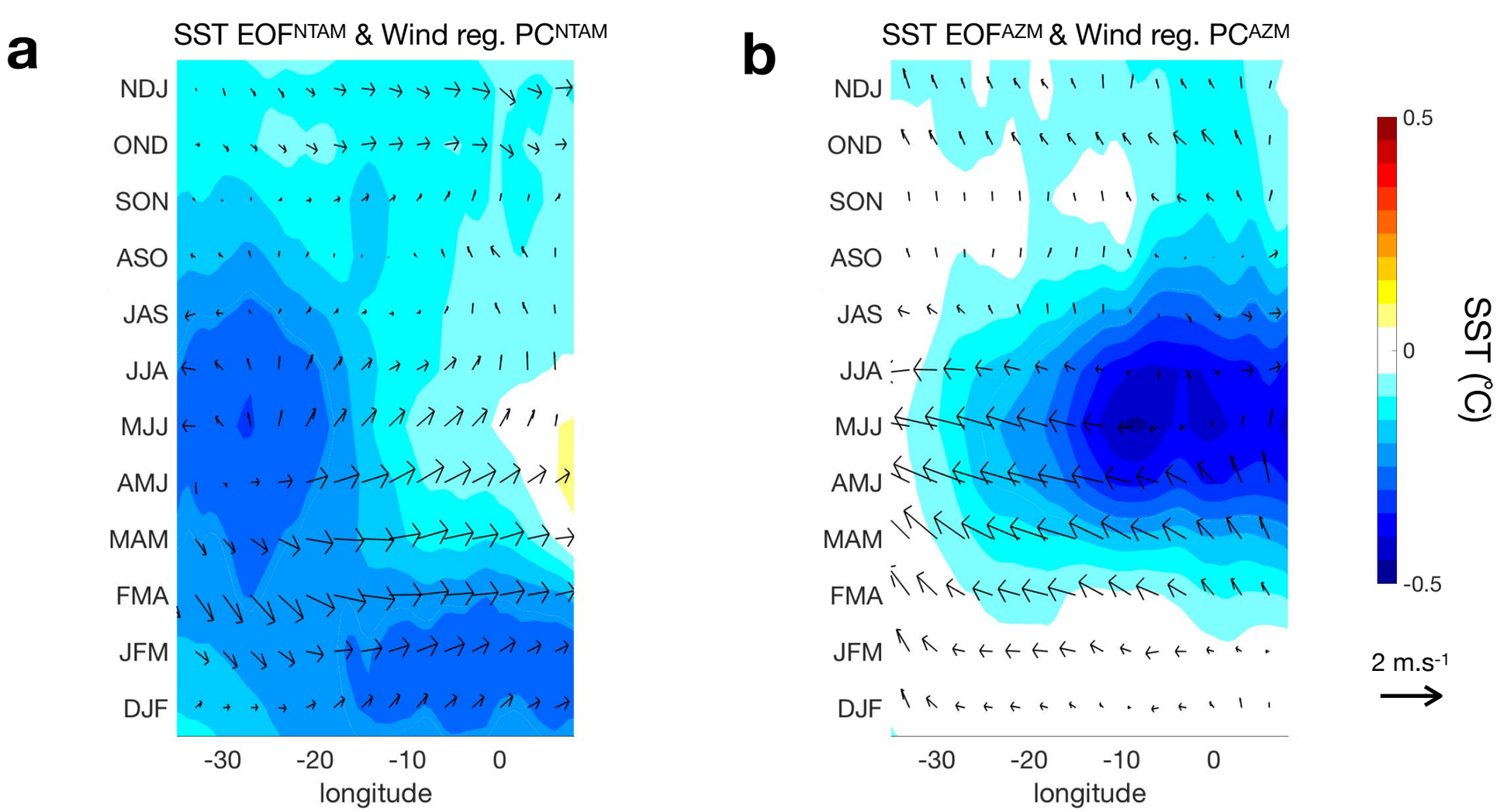

Figure 4: Phenology of equatorial surface properties associated with NTAM (left panels) and AZM (right panels) EOF modes of JJA interannual Tropical Atlantic SSTA. 3-month running-mean of SST, surface wind, SSH, and Chl-a interannual anomalies from preceding winter (DJF) to following winter (NDJ) are regresses onto the standardized PCs (shown in Fig.3ef) and averaged within [3˚S-3˚N]. SSTA (color shading, °C) and surface winds anomalies (arrows, m.s-1) associated with JJA NTAM and AZM are displayed on top panels. On bottom panels, same for Chl-a (color shading, mg.m-3) and SSH (contours, cm) interannual anomalies.